A compact complex-coefficient microwave photonic filter with continuous tunability

Jinwang Qian (钱金旺), Zhennan Zheng (郑桢楠), Mingzheng Lei (雷明政), Chunqi Song (宋春奇), Shanguo Huang (黄善国)*, and Xinlu Gao (高欣璐)**

State Key Laboratory of Information Photonics and Optical Communications, Beijing University of Posts and Telecommunications, Beijing 100876, China

**Corresponding author: shghuang@bupt.edu.cn; **corresponding author: xinlugao@bupt.edu.cn*

Received April 19, 2019; accepted July 26, 2019; posted online August 27, 2019

A complex-coefficient microwave photonic filter with continuous tunability is proposed and demonstrated, which has a compact structure and stable performance without splitting the optical path and tuning the polarization state. By only controlling the DC biases of the modulator, the amplitudes and the phases of the filter taps can both be tuned. The phase difference between the two filter taps covers a full 360° range from 10 GHz to 32 GHz. Frequency responses of the proposed filter are measured within 10–20 GHz with different center frequencies.

OCIS codes: 060.5625, 070.2615, 050.5080.

doi: 10.3788/COL201917.100601.

A microwave photonic filter (MPF) can find potential applications in microwave signal processing, communication, radar, and so on, due to its inherent advantages of wideband, tunability, reconfigurability, and immunity to electromagnetic interference[1–3]. To avoid optical interference and overcome the impact of the environment vibration, various MPFs implemented in the incoherent regime have been proposed[1–18]. In Refs. [4–6], the tap coefficients of these filters are all positive. However, an all-positive-coefficient MPF is a low-pass filter. To achieve the band-pass filtering function, MPFs with negative coefficients[7–10] and complex coefficients[11–16] are proposed. The tunability of these negative-coefficient MPFs is realized by changing the time delay differences between the filter taps, resulting in performance deterioration, such as undesirable changes of the free spectral range (FSR) and the filtering shape. Complex-coefficient MPFs are able to maintain the FSR when the center frequency is changed, so they have the most potential for applications among the MPFs with different coefficients. The principle to achieve the complex coefficients is to introduce phase shifts between different taps, which can be realized by single-sideband (SSB) modulation[11], polarization modulation[12], a wideband 90° hybrid coupler (HC)[13], a dual-parallel Mach–Zehnder modulator (DPMZM)[14], or a programmable wavelength processor[15]. However, these schemes use two or more optical sources, making the system costly and complex. For example, in Refs. [13] and [14], both of them are two-tap filters with one tap having a real positive coefficient and the other tap having a complex coefficient. Each tap needs one laser source and one modulator. Reference [16] proposed a complex-coefficient MPF based on polarization modulation with one single optical source. Such a structure is less complex. By controlling a polarization controller (PC), phase offset of the recovered microwave signals between the two taps covers a full 360° range so that the filter is tunable over the full FSR. However, due to polarization state being sensitive to the environment, the phase shift is not very stable in the schemes[16–18] by tuning the PC to shift the phase. Meanwhile, since the PC is controlled manually and not easy to adjust, the accuracy and the speed of phase tuning are low. Reference [19] proposed a microwave photonic phase shifter (MPPS) by using a DPMZM and a tunable optical band-pass filter (TOBPF). Instead of by controlling a PC, the radio frequency (RF) phase shift is realized by simply tuning the bias voltage of the modulator. A continuous phase shift with good stability and small power variation is achieved within a wide bandwidth.

In this Letter, we propose and demonstrate a two-tap MPF, with each tap having a complex coefficient, which is simple, easily tunable, and stable. The complex coefficients are based on two MPPSs[19], which can be realized by a dual-polarization quadrature phase shift keying (DP-QPSK) modulator and an optical band-pass filter (OBPF). After the RF modulation and removing one sideband by the OBPF, two SSB signals with orthogonal polarizations are generated. The detection of the two orthogonally polarized SSB signals at the photodetector (PD) is incoherent. Thus, two independently tunable RF phase shifters based on Ref. [19] are obtained with one single modulator, forming the two filter taps. Instead of splitting the optical path to introduce different time delays to the two filter taps, a tunable differential group delay element (TDGDE) is used without splitting the optical path. By only controlling the DC biases of the DP-QPSK modulator to change the phase shift difference between the filter taps, the center frequency of the proposed MPF is tunable over the full FSR without affecting the FSR. Meanwhile, the FSR can be changed by tuning the time delay between the two taps, which can be realized by adjusting the TDGDE to change the time delay

between the two taps. The proposed scheme utilizes only one optical source and one modulator. Without splitting the optical path and tuning the polarization state, the structure is more compact and more stable compared with the schemes[16–18] by tuning the PC to shift the RF phase. A proof-of-concept experiment is conducted. Experimental results show that the proposed filter has good stability and continuous tunability.

Figure 1(a) shows the structure of the proposed tunable complex-coefficient MPF. The optical carrier (OC) emitted by a laser diode (LD) is launched into the DP-QPSK modulator. The detailed structure of the DP-QPSK modulator is shown in the dash box in Fig. 1(a). It integrates two parallel quadrature phase shift keying (QPSK) modulators, whose polarization states are orthogonal polarizations[20]. The OC is split in half into the two QPSK modulators. Figure 1(b) shows the detailed structure of the QPSK modulator. Each QPSK modulator has two parallel Mach–Zehnder modulators (MZM1 and MZM2) to modulate the input microwave signal and a third MZM (MZM3) to shift the optical signal phase. An RF signal generated by a vector network analyzer (VNA) is separated into two branches with equal power after the HC. The RF signals in the two branches are modulated by the lower MZMs (MZM2) of the two QPSK modulators, respectively. The two MZMs driven by the RF signal are biased at the minimum transmission point (MITP) to conduct the carrier-suppressed dual-sideband (CS-DSB) modulation. The other two MZMs without a driven signal are biased at the maximum transmission point (MATP) to let the OC pass through. Each QPSK modulator outputs a CS-DSB+OC signal, as shown in Fig. 1(b). By controlling the DC bias of MZM3, the phase difference between the CS-DSB signal and the OC can be tuned. The signals from the two QPSK modulators are mapped orthogonally in two polarizations. Suppose the OC and two RF signals are expressed as $\exp(j\omega_c t)$ and $V_m \cos(\omega_m t + \phi_i)(i = 1, 2)$, respectively, where ω_c is the angular frequency of the OC, and V_m, ω_m, and ϕ_i are the magnitude, angular frequency, and phase of the RF signal, respectively. The output optical field of the DP-QPSK modulator is expressed as[17]

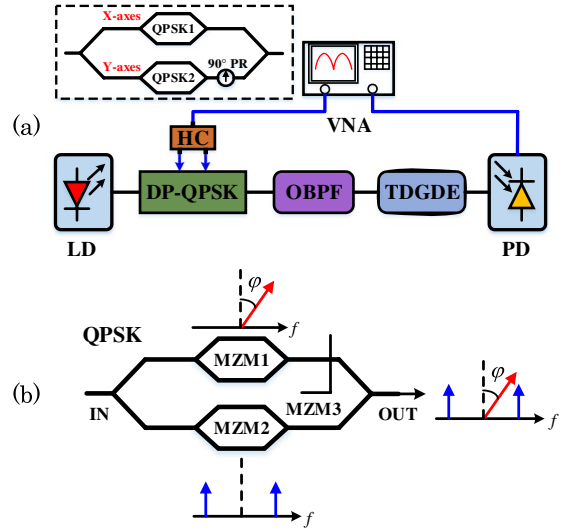

Fig. 1. (a) Proposed tunable MPF. LD, laser diode; VNA, vector network analyzer; DP-QPSK modulator, dual-polarization quadrature phase shift keying modulator; HC, hybrid coupler; OBPF, optical band-pass filter; TDGDE, tunable differential group delay element; PD, photodetector; 90° PR, 90° polarization rotator. (b) The detailed structure of the QPSK modulator. MZM, Mach–Zehnder modulator.

$$\begin{bmatrix} E_x \\ E_y \end{bmatrix} = \frac{1}{\sqrt{2}} \exp(j\omega_c t) \times \begin{bmatrix} \cos[\beta \cos(\omega_m t + \phi_1) + \varphi_1/2] + \cos(\varphi_2/2) \exp(j\varphi_3) \\ \cos[\beta \cos(\omega_m t + \phi_2) + \varphi_4/2] + \cos(\varphi_5/2) \exp(j\varphi_6) \end{bmatrix}, \tag{1}$$

where E_x and E_y are the signals in the two principal axes of the DP-QPSK modulator, respectively, $\beta = \pi V_m / V_\pi$ is the modulation index, V_π is the half-wave voltage of the sub-MZM at microwave frequency, and $\varphi_l = \pi V_l / V_{\pi-bias}$ $(l = 1, 2, 3, 4, 5, 6)$ is the static phase shift controlled by the DC bias. Among them, φ_3 and φ_6 are the phase differences between the CS-DSB signal and the OC, V_l is the bias voltage, and $V_{\pi-bias}$ is the static half-wave voltage of the sub-MZM at DC. Tune the bias voltages to achieve $\varphi_1 = \varphi_4 = \pi$. Applying the Jacobi–Anger expansion and considering small signal modulation only, Eq. (1) can be expanded as

$$\begin{bmatrix} E_x \\ E_y \end{bmatrix} = \frac{1}{\sqrt{2}} \begin{bmatrix} -J_1(\beta)\left\{\exp[j(\omega_c t + \omega_m t + \phi_1)] + \exp[j(\omega_c t - \omega_m t - \phi_1)]\right\} + \cos(\varphi_2/2)\exp[j(\omega_c t + \varphi_3)] \\ -J_1(\beta)\left\{\exp[j(\omega_c t + \omega_m t + \phi_2)] + \exp[j(\omega_c t - \omega_m t - \phi_2)]\right\} + \cos(\varphi_5/2)\exp[j(\omega_c t + \varphi_6)] \end{bmatrix}, \tag{2}$$

where $J_1(\beta)$ is the first-order Bessel function of the first kind.

An OBPF is used to remove one RF modulation sideband. At the output of the OBPF, two SSB signals with orthogonal polarizations are generated, as

$$\begin{bmatrix} E_x \\ E_y \end{bmatrix} = \frac{1}{\sqrt{2}} \begin{bmatrix} -J_1(\beta)\exp[j(\omega_c t + \omega_m t + \phi_1)] + \cos(\varphi_2/2)\exp[j(\omega_c t + \varphi_3)] \\ -J_1(\beta)\exp[j(\omega_c t + \omega_m t + \phi_2)] + \cos(\varphi_5/2)\exp[j(\omega_c t + \varphi_6)] \end{bmatrix}. \tag{3}$$

When the signals in Eq. (3) are injected into the PD, two electrical currents are obtained:

$$i_{RF1}(t) \propto J_1(\beta)\cos(\varphi_2/2)\cos(\omega_m t + \phi_1 - \varphi_3), \tag{4}$$

$$i_{RF2}(t) \propto J_1(\beta)\cos(\varphi_5/2)\cos(\omega_m t + \phi_2 - \varphi_6). \tag{5}$$

Since $\varphi_l = \pi V_l / V_{\pi-bias}\,(l = 2, 3, 5, 6)$ can be tuned from 0 to 2π by controlling the DC bias of the sub-MZM, the two recovered RF signals can realize a full 360° phase shift, and the powers of them can be changed.

The signals after the OBPF propagate through a TDGDE. The principal axes of the TDGDE and the DP-QPSK modulator are aligned to each other. TDGDE introduces different time delays to E_x and E_y. The two SSB signals are detected at the PD in the incoherent regime. The recovered RF signal after the PD is a summation of $i_{RF1}(t)$ and $i_{RF2}(t)$, as

$$\begin{aligned} i(t) &= i_{RF1}(t) + i_{RF2}(t) \\ &\propto \sum_{n=1}^{2} a_n \cos[\omega_m t + \theta_n + \omega_m (n-1) T], \end{aligned} \tag{6}$$

where $a_n \propto J_1(\beta)\cos(\varphi_l/2)\,(l = 2, 5)$ is the output power in the nth tap, which can be changed by controlling the DC bias of the corresponding sub-MZM; $\theta_n = \phi_i - \varphi_l\,(i = 1, 2,\ l = 3, 6)$ is the RF phase shift in the nth tap, which can be shifted from 0 to 2π by controlling the DC bias of the third MZM (MZM3); T is the differential time delay between E_x and E_y.

The transfer function of the proposed two-tap MPF is expressed as

$$H(\omega_m) \propto a_1 + a_2 \exp(j\omega_m T)\exp(j\Delta\theta), \tag{7}$$

where $\Delta\theta$ is the phase shift difference between the two recovered RF signals.

Compared with the transfer function of conventional two-tap positive-coefficient MPF[21], which is

$$H'(\omega_m) \propto a_1 + a_2 \exp(j\omega_m T), \tag{8}$$

the proposed filter in Eq. (7) has a complex coefficient. The frequency response of the proposed MPF can be rewritten as

$$H(f) = H'(f + \Delta\theta/2\pi T), \tag{9}$$

where f is the frequency of the RF signal; $\Delta\theta/2\pi T$ is the change of the center frequency, which can be tuned by controlling the DC bias of the DP-QPSK modulator. The proposed filter is tunable over the full FSR, since the phase shift covers a full 360° range. Moreover, by tuning the DGD of the TDGDE, the FSR can be changed. The two-tap filter shown in Fig. 1 can be extended to a multi-tap filter by adding more optical sources and modulators. A system with N optical paths formed by the proposed structure will generate $2 \times N$ taps.

Based on the setup shown in Fig. 1, a proof-of-concept experiment is implemented. An 8.0 dBm OC at ~1550.0 nm emitting from a tunable laser source (TLS) is fed to the DP-QPSK modulator (Fujitsu FTM7977HQA). The linewidth of the OC is ~100 kHz. A −25 dBm RF signal with the frequency of 20 GHz generated by the VNA (Agilent 8722ES) is amplified by a broadband electrical amplifier (OA4MVM3), which has a wide frequency range from 30 kHz to 45 GHz and a gain of 27 dB. The amplified RF signal is divided in half into two branches by a 0° power divider. We define the bias voltages of each sub-MZM as X1, X2, X3, Y1, Y2, and Y3, where X and Y represent the X axes and Y axes, 1, 2, 3 represent MZM1, MZM2, and MZM3 of the QPSK modulator in the X axes and Y axes[22]. One branch of the amplified RF signal is used to drive the lower MZM (MZM2) of the QPSK modulator in the X axes. When X1, X2, Y1, Y2 are all biased at the MITP, the DP-QPSK modulator outputs a CS-DSB signal, as the black curve shown in Fig. 2(a). When X1 is changed to bias at the MATP, the DP-QPSK modulator generates a CS−DSB+OC signal, as the red curve shown in Fig. 2(a). The OC is eliminated more than 40 dB. The CS−DSB+OC signal is sent to a waveshaper (Finisar

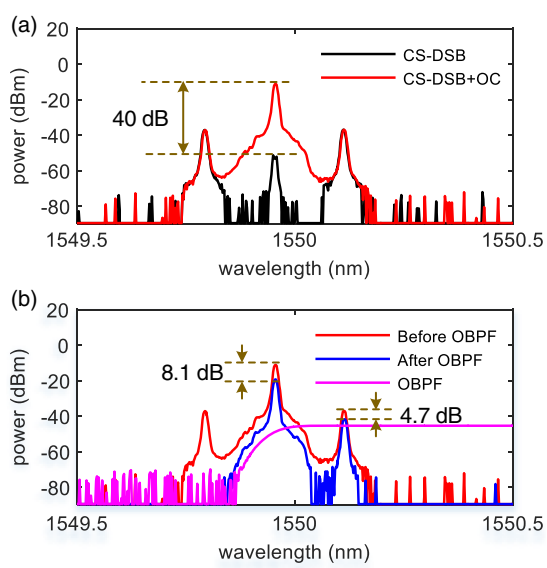

Fig. 2. (a) Measured optical spectra of the CS-DSB and CS−DSB+OC signal. (b) Measured optical spectra before and after the OBPF, as well as the transfer function of the OBPF.

Waveshaper 4000 s), which is a polarization-independent and programmable optical spectrum processor[23,24]. The waveshaper is used as an OBPF to eliminate the upper frequency sideband. Figure 2(b) shows the measured optical spectra before and after the OBPF, as well as the transfer function of the OBPF.

We measure the phase shift property of the MPPS by only using the QPSK modulator in the X axes. The obtained optical SSB signal after the OBPF, as the blue curve shown in Fig. 2(b), is amplified by an erbium-doped fiber amplifier (EDFA, Conquer KG-EDFA-P). The output power of the EDFA is about 3.1 dBm. The amplified optical signal is detected by a PD (Optilab PD30). The power frequency response and phase frequency response of the recovered RF signal can be measured by sending it back to the VNA. The phase shifts of the RF signal within 10–32 GHz are recorded from −180° to 180° with the step of 45° by tuning the voltage of X3, as shown in Fig. 3(a). It indicates that the RF phase shift is unconcerned with the frequency. The frequency response of the MPPS is almost flat over a wide bandwidth. The minimum frequency is limited by the slope property of the OBPF, and the maximum frequency is limited by the PD. Figure 3(b) shows that the relative power variation is within ±1 dB for different phase shifts. The phase shifter shows a good stability performance over a wide bandwidth. Figure 4 shows the phase shift and the relative power variation of the RF signal at the frequency of 20 GHz over the sweeping time of 200 s. Results show that the MPPS has good long-term stability. The phase shift property of the MPPS by only using the QPSK modulator in the Y axes is also measured with the same procedure. Results also show good phase shift performance, which is consistent with the above results. Therefore, it is possible to implement a complex-coefficient MPF based on these two tunable MPPSs.

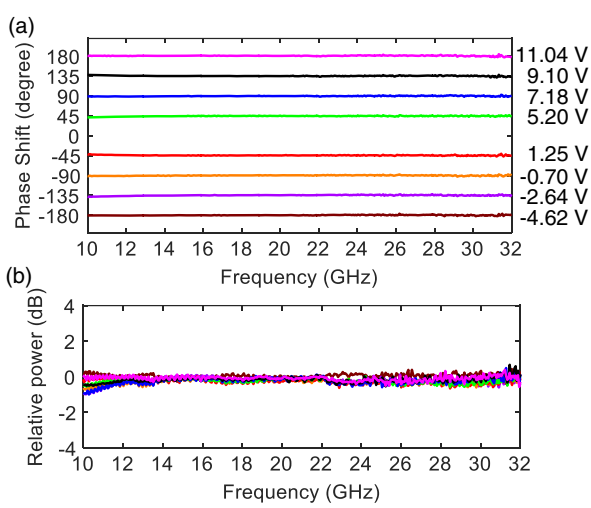

Fig. 3. (a) Phase shift of the recovered RF signal over the frequency range of 10–32 GHz. (b) Relative power variation for different phase shifts.

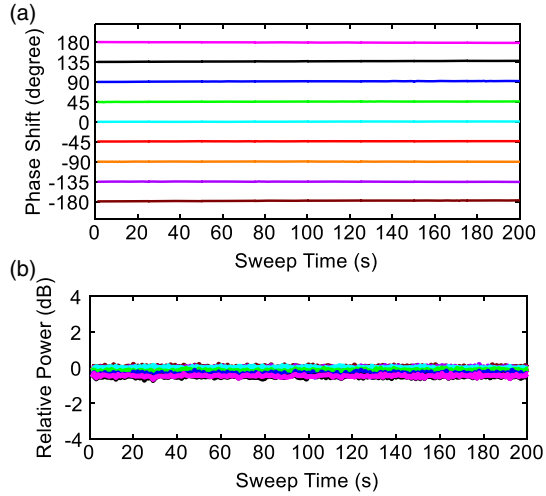

Fig. 4. Measured (a) phase shift and (b) relative power variation of the RF signal at the frequency of 20 GHz over the sweeping time of 200 s.

When X1, Y1 are biased at the MATP, X2, Y2 are biased at the MITP, and the RF signals in the two branches are applied to the lower MZMs (MZM2) of the two QPSK modulators, respectively; two MPPSs are realized using one DP-QPSK modulator and one polarization-independent OBPF. Since the modulated signal generated by the two QPSK modulators is polarized orthogonally, these two phase shifters are independently tunable by controlling the corresponding DC biases. In order to implement a two-tap MPF, a TDGDE is used after the OBPF to introduce different time delays to the two orthogonally polarized SSB signals. Lack of an available TDGDE, we use a polarization maintaining fiber (PMF) with the length of ~300 m to accomplish a validating experiment. The principal axes of the PMF and the DP-QPSK modulator are aligned to each other by adjusting the PC. After the alignment, the polarization state is fixed, and there is no need to tune the PC. The two orthogonally polarized SSB signals go through different time delays and then interfere at the PD in the incoherent regime. The frequency response of the obtained two-tap MPF is measured by the VNA. Because the two recovered RF signals at each tap are equivalent, and both of them can achieve a full 360° phase shift, we only need to change their phase difference to realize the center frequency tuning. We adjust the bias voltage of X3 to shift the RF phase. Figure 5 shows the measured frequency responses of the proposed filter from 10 GHz to 20 GHz. By tuning the voltage of X3 from −4 V to +8 V with steps of 4 V, the frequency responses with different center frequencies are obtained, as shown in Fig. 5(a). The FSR is maintained at 2.1 GHz when the center frequency is tuned. Figure 5(b) shows the frequency responses within 20 min with intervals of 2 min. Results show good long-term stability for the center frequency and shape of the proposed MPF. Figure 6 shows the position changes for two adjacent notches of the filter by tuning the voltage

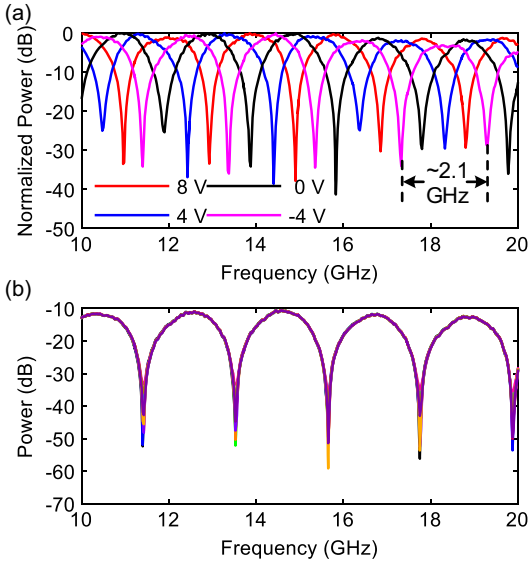

Fig. 5. Measured frequency responses of the proposed MPF (a) with different bias voltages of X3 and (b) at different times with the same bias voltages.

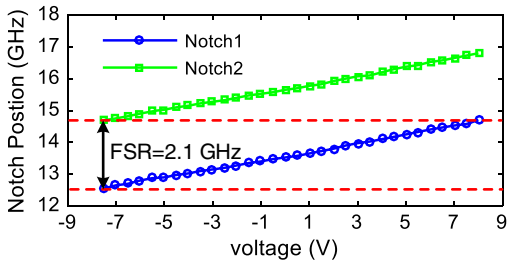

Fig. 6. Measured notch positions of the proposed filter with different bias voltages.

of X3 from −7.5 V to +8 V with steps of 0.5 V. It indicates that the center frequency of the proposed MPF is continuously tunable over the full FSR. The change of the notch position is nearly linear with the change of the bias voltage, which agrees well with the theoretical analysis. The imperfection of the linearity is due to the frequency interval of the measured frequency response being 0.025 GHz.

In conclusion, we propose and demonstrate a continuously tunable complex-coefficient MPF based on a DP-QPSK modulator and an OBPF. This structure uses a TDGDE to introduce relative time delay between two filter taps, which makes it compact and stable without splitting the optical path and tuning the polarization state. By controlling the DC biases of the DP-QPSK modulator, the center frequency of the proposed MPF is tunable without affecting the FSR. Frequency responses of the proposed MPF are measured within 10–20 GHz with an FSR of 2.1 GHz. Experimental results show good long-term stability for the center frequency and shape of the proposed MPF.

This work was supported by the National Natural Science Foundation of China (NSFC) (Nos. 61690195, 61575028, 61605015, 61622102, 61821001, and 61801038).

References

1. J. Capmany, B. Ortega, and D. Pastor, J. Lightw. Technol. **24**, 201 (2006).
2. J. Yao, IEEE Microw. Mag. **16**, 46 (2015).
3. R. A. Minasian, IEEE Trans. Microw. Theory Tech. **54**, 832 (2006).
4. J. Capmany, D. Pastor, and B. Ortega, IEEE Trans. Microw. Theory Technol. **47**, 1321 (1999).
5. Y. Jin, X. Dong, J. Zhou, and P. P. Shum, Microw. Opt. Technol. Lett. **53**, 123 (2011).
6. J. Mora, B. Ortega, A. Díez, J. L. Cruz, M. V. Andrés, J. Capmany, and D. Pastor, J. Lightw. Technol. **24**, 2500 (2006).
7. J. Capmany, D. Pastor, A. Martinez, B. Ortega, and S. Sales, Opt. Lett. **28**, 1415 (2003).
8. T. Y. Kim, C. K. Oh, S. J. Kim, and C. S. Park, IEEE Photon. Technol. Lett. **19**, 907 (2007).
9. J. Yao and Q. Wang, IEEE Photon. Technol. Lett. **19**, 644 (2007).
10. M. Wang and J. Yao, IEEE Photon. J. **5**, 5500709 (2013).
11. M. Sagues, A. Loayssa, J. Capmany, D. Benito, S. Sales, and R. Garcia-Olcina, in *Conference on Optical Fiber Communication & National Fiber Optic Engineers Conference* (2007), paper OWU5.
12. Y. Zhang and S. Pan, Opt. Lett. **38**, 802 (2013).
13. Y. Yan and J. Yao, IEEE Photon. Technol. Lett. **19**, 1472 (2007).
14. W. Li, N. Zhu, and L. Wang, IEEE Photon. J. **3**, 462 (2011).
15. X. Yi, T. X. H. Huang, and R. A. Minasian, IEEE Trans. Microw. Theory Tech. **58**, 3088 (2010).
16. C. Zhang, L. Yan, W. Pan, B. Luo, X. Zou, H. Jiang, and B. Lu, IEEE Photon. J. **5**, 5501606 (2013).
17. Y. Zhang and S. Pan, Opt. Lett. **42**, 5035 (2017).
18. S. Zhu, M. Li, X Wang, N. Zhu, and W. Li, Opt. Commun. **431**, 11 (2019).
19. J. Shen, G. Wu, W. Zou, and J. Chen, Appl. Phys. Express **5**, 072502 (2012).
20. X. Li, S. Zhao, Z. Zhu, K. Qu, T. Lin, and S. Pan, Chin. Opt. Lett. **15**, 070603 (2017).
21. Y. Zhang and S. Pan, IEEE Photon. Technol. Lett. **25**, 188 (2013).
22. W. Wang, J. Liu, H. Mei, and N. Zhu, Opt. Express **24**, 395 (2016).
23. X. Gao, M. Zhao, M. Xie, M. Lei, X. Song, K. Bi, Z. Zheng, and S. Huang, Opt. Lett. **44**, 257 (2019).
24. M. Lei, Z. Zheng, J. Qian, M. Xie, X. Gao, and S. Huang, IEEE Photon. J. **11**, 5500711 (2019).